A Comparative Study of Methanol Adsorption and Dissociation over $WO_3(001)$ and $ReO_3(001)$

A comparative study of methanol adsorption and dissociation over WO_3(001) and ReO_3(001)

Qingfeng Ge[*] and Maciej Gutowski[§,%]

[*]Department of Chemistry and Biochemistry, Southern Illinois University, Carbondale, IL 62901. [§]Chemical Sciences Division, Fundamental Sciences Directorate, Pacific Northwest National Laboratory, P.O. Box 999, Richland, WA 99352. [%]Institute of Chemical Sciences, School of Engineering and Physical Sciences, Heriot-Watt University, Edinburgh, EH14 4AS, United Kingdom

Corresponding author: Prof. Qingfeng Ge, Department of Chemistry and Biochemistry, Southern Illinois University, Carbondale IL 62901

Tel: 618 453 6406

Email addresses: qge@chem.siu.edu; m.gutowski@hw.ac.uk

Abstract

Tungsten ($5d^4 6s^2$) and rhenium ($5d^5 6s^2$) form MO_3 oxides (M = W or Re) with similar structures. The adsorption and dissociation of methanol on these oxide surfaces, often used to probe the surface redox centers, have been analyzed using periodic density functional calculations. Molecular adsorption of methanol at the metal site on both surfaces with 0.5 ML oxygen coverage was found to be exothermic with adsorption energies of -74 and -106 kJ/mol on WO_3(001) and ReO_3(001), respectively. In contrast, heterolytic dissociation of methanol to adsorbed methoxide species at the metal site and H at the surface oxygen site is not energetically favored on WO_3(001) but favored on ReO_3(001). The dissociation energies to form coadsorbed methoxide and hydrogen adatom are 35 kJ/mol on WO_3 and -112 kJ/mol on ReO_3, respectively. The activation barrier for dissociating the molecularly adsorbed methanol on ReO_3(001) was determined to be 19 kJ/mol. Dehydrogenation to form coadsorbed hydroxymethyl and hydrogen adatom is not energetically favorable on both surfaces with respect to the molecularly adsorbed methanol. However, the dehydrogenation path is exothermic with respect to the gas phase methanol on ReO_3, with the heats of reaction of -25 kJ/mol, but highly endothermic on WO_3, with the heats of reaction of 114 kJ/mol.

Keywords: Transition metal oxides; Methanol; Dissociation; Dehydrogenation; DFT

1. Introduction

Transition metal oxides are widely used as both catalysts and supports of catalyst.[1] For example, supported WO_x catalysts have been used in hydrocarbon cracking,[2] isomerization of alkenes and alkanes,[3-6] olefin metathesis,[7] and selective catalytic reduction of NO_x.[8] Supported rhenium oxides were found to catalyze the oxidation of methanol to dimethoxymethane and selective oxidation of propane.[9, 10] The performance of these oxides as either catalysts or supports of catalyst is strongly dependent on their intrinsic properties and structure of the exposing surfaces. Understanding the nature of transition metal oxides and the molecular interactions on the surfaces of oxides is therefore important to optimize the reactivity and selectivity of existing catalysts and to design new catalytic systems with improved performance.

Methanol is a commodity and has been proposed as a primary target molecule for CO_2 hydrogenation as well as CO_2 electrochemical reduction.[11, 12] It can be selectively oxidized over many transition metal oxides to products such as formaldehyde and methyl formate which are important primary reagents for organic synthesis.[13] The product distribution of the selective oxidation reaction depends on the nature of oxides. Methanol can also be used as an alternative fuel or an on-board carrier of hydrogen for hydrogen fuel cell powered vehicles.[14] In addition, methanol has been proposed as a probe molecule to analyze the number as well as the nature of surface active sites on many transition metal oxide catalysts.[15] Wachs and coworkers have suggested that the oxygen bridging the support metal atom to the V=O center over supported vanadia catalysts plays an important role in the selective oxidation of methanol based on the dependence of turnover frequency on the nature of the support.[16-18] These authors proposed the following simple mechanism:

$$CH_3OH+V\text{-}O\text{-}M \leftrightarrow CH_3O\text{-}V+M\text{-}O\text{-}H \qquad (R1)$$

$$CH_3O\text{-}V+O_{ad} \rightarrow CH_2O+V\text{-}OH \qquad (R2)$$

$$M\text{-}O\text{-}H+V\text{-}OH \leftrightarrow H_2O+V\text{-}O\text{-}M \qquad (R3)$$

Reaction (R1) represents protonation of the V-O-M bond followed by M-O-V bond scission and CH_3O^- addition to vanadium. The reactions that follow include methoxide dissociation (R2) and disproportionation reaction of surface hydroxyls (R3). A number of mechanistic models have been developed, including attempts to evoke the role of the electronegativity of the cations in the support and the modes in which various bridging O atoms are activated. This mechanism has

been expanded to explicitly incorporate oxygen vacancy formation and filling, and alteration of charge on the metal cations.

The structurally similar oxides of tungsten and rhenium offered an opportunity to probe the effect of the charges on the cations to their reactivity toward methanol. A difference by one 5d electron between rhenium ($5d^5 6s^2$) and tungsten ($5d^4 6s^2$) has significant consequences on the properties of their trioxides MO_3 (M = W or Re). For example, ReO_3 is cubic with a perovskite-like structure,[19] but the structure of WO_3 is distorted through tilting the WO_6 octahedra and displacing the W atoms from the octahedral centers.[19, 20] The stoichiometric WO_3 is a semiconductor with a band gap of 2.6 eV.[21] ReO_3, however, has one extra electron in the valance shell of each metal atom and the resulting band is only partially filled. Indeed, the conductivity of ReO_3 reaches 10^7 Ωcm^{-1} at low temperatures.[22] Due to their unique electronic/redox properties, nanostructured tungsten and rhenium oxides have been found applications in gas sensing and catalysis.[23] We studied the chemistries of methanol on the surfaces of CeO_2,[24, 25] Pt/TiO_2[26] and PdIn.[27] In the present paper we focus on whether differences in electronic and crystal structure of WO_3 and ReO_3 contribute to differences in chemical properties of the (001) surfaces of these trioxides. In particular we investigate adsorption and dissociation of methanol on these two surfaces.

2. Computational Details

Periodic DFT calculations reported herein were performed using the Vienna Ab initio Simulation Package (VASP).[28, 29] VASP is a plane wave code with ultrasoft pseudopotential[30] or projector augmented wave (PAW)[31, 32] to describe nuclei and core electrons. Gradient-corrected exchange-correlation functionals, PW91[33] and PBE[34] have been tested and the differences in the energetics and structures of using the two types of functionals were found to be negligible if the calculations were done self-consistently, i.e. using the PAW or pseudo-potentials generated with the same exchange-correlation functionals. As such, PAW potentials and PBE functionals were chosen in the present calculations. The 5d and 6s valence states of W and Re were treated explicitly in the calculations. The effect of treating the semi-core 5p state explicitly for W and Re was found negligible for the properties considered here. Spin-polarization was included in calculations when it became necessary. Test calculations using a cutoff energy up to 600 eV showed that the plane wave basis is converged to within 0.02

Å for relaxed bond distances and 0.05 eV for adsorption energies at 400 eV. A Gaussian type of electronic smearing with a width of 0.1 eV was used to improve convergence of electronic self-consistent cycles. For bulk and surface calculations, Monkhorst-Pack[35] scheme was used to generate k-points to sample the Brillouin zone. A space of less than 0.05 $Å^{-1}$ between two adjacent k-points in any directions was found to be appropriate for these oxides. In the studies of oxygen coverage effect, two-sided slabs with 6 layers of metal atoms were adopted. In the simulation of methanol adsorption and dissociation, we used a one-sided approach, i.e., placing methanol or the dissociative products on one side of the slab. The calculated adsorption energy of methanol on WO_3(001) is only different by 0.04 eV from that calculated with a two-sided model. The vacuum space between the adjacent slabs was kept larger than 12 Å. The adsorbate atoms as well as the W (or Re) and O atoms in the top 3 triple layers were optimized according to the forces calculated quantum mechanically. The geometries were relaxed using a conjugate-gradient or quasi-Newton scheme as implemented in VASP. A geometry optimization was considered converged when the maximum force on the movable atoms reaches 0.05 eV/Å or less. Transition state search was carried out by using the nudged elastic band (NEB) method and its improvements developed by Jonsson and co-workers.[36-38] Transition states determined with NEB were further optimized by quasi-Newton algorithm to minimize forces on the movable atoms.[39, 40] Normal mode harmonic vibrational analysis has been performed for the transition states and for selected adsorption geometries using the finite difference method as implemented in the latest version of VASP.[41]

3. Results and Discussion

Bulk ReO_3 has a perovskite cubic structure with an experimental lattice constant of 3.747 Å at 100 K and 3.748 Å at 300 K.[42] On the other hand, bulk WO_3 exhibits a series of polymorphs which can be considered as distortion of the ideal cubic ReO_3 structure. The monoclinic unit cell of ε-WO_3 can be approximated by a reconstructed orthorhombic cell based on a cubic ReO_3 cell scaled by ($\sqrt{2}\times\sqrt{2}\times2$). The low temperature ε-WO_3 phase has a lattice constant of a=5.278 Å, b=5.156 Å, c=7.664 Å and β=91.762° as measured in neutron powder diffraction experiment.[43] Using these experimentally determined structures as input, we optimized the bulk structures of both ReO_3 and WO_3. ReO_3 remains a perfect cubic structure after relaxation and the equilibrium lattice constant is 3.767 Å, in good agreement with the experimental results.[42] The optimized

lattice parameters of the ε-WO_3 phase are a= 5.274 Å, b= 5.130 Å, c=7.638 Å and β=92.243˚, also in good agreement with the experiment.[43] The two W-O bonds to the same W atom along c-axis are 1.777 and 2.149 Å, respectively. The relaxed bulk WO_3 and ReO_3 structures were shown in fig. 1 in octahedron representations. In order to compare with WO_3, we constructed a ($\sqrt{2}\times\sqrt{2}\times2$) unit cell for ReO_3 on the basis of the cubic structure. The distortion of the ε-WO_3 structure from the perfect cubic structure as represented by ReO_3 can be clearly identified by comparing the structures shown in fig. 1(a) for WO_3 and fig. 1(b) for ReO_3. These relaxed bulk structures were subsequently used to create the slabs to simulate the surface as well methanol adsorption and dissociation.

There are different ways to build the (001) surface of WO_3 and ReO_3. The surface may be terminated by either O or WO_2 (ReO_2). The surface may also be partly covered with oxygen. We analyzed different possibilities for the surfaces of both oxides and present the results for WO_3(001) and ReO_3(001) in turn in the following sections.

3.1 WO_3 (001)

We started from a slab with a c(2×2) surface unit cell, terminated by WO_2 on both sides. The slab so-formed is non-polar and also non-stoichiometric. The surface with such a composition can only exist in a highly reducing environment. If we add an oxygen atom in the unit cell on each side of the slab, we can make the slab stoichiometric and keep it non-polar. Consequently, the W atoms of the half surface WO_2 units will be covered by the oxygen atoms. The oxygen atoms form a c(2×2) super structure as shown by the blue box in figure 2(a). The formation of the c(2×2) oxygen super structure on WO_3(001) is highly exothermic. The integral heats of dissociative adsorption is -603.8 kJ/mol. Increasing the oxygen coverage to a full monolayer, i.e., covering all the W atoms of the slab with oxygen, the integral heats of dissociative adsorption are still negative with respect to the WO_2 terminated slab and isolated O_2 molecules, with a value of -78.2 kJ/mol. We note, however, much of the contribution to the negative integral heats at 1 ML oxygen coverage came from occupying the first half of surface W atoms. In fact, the O_2 dissociative adsorption energy becomes 448.5 kJ/mol if the 0.5 ML oxygen covered stoichiometric slab was used as a reference. These results indicate that WO_3(001) surfaces with either pure O or pure WO_2 termination are not stable. The stable configuration corresponds to a surface with 0.5 ML oxygen coverage.[44] This is in general agreement with the experimental

findings from LEED and STM measurements.[45, 46] The striking difference of oxygen binding energies on two surface WO_2 units can be attributed to the nonequivalent surface W atoms to which the oxygen atoms bind directly. In general, the W-O bond lengths along the surface normal alternate between long and short. This effect was propagated to the surface: the half strongly bonded oxygen happens to occupy the W site, which will form a shorter W-O bond on the surface. Terminating the surface with WO_2 makes the W-O bonds to the subsurface oxygen almost uniform. Adding 0.5 ML oxygen on the W site corresponding to the shorter W-O bond recovers the "long-short" pattern of W-O bond lengths in bulk WO_3 along the c-axis and the terminal O-W bond is 1.71 Å. In fact, if oxygen occupies the "wrong" W site, the adsorption energy will be reduced to -162.1 kJ/mol even at 0.5 ML oxygen coverage.

The results of spin-polarized calculations for all three cases: WO_2-terminated, 0.5 and 1 ML oxygen covered slabs, showed that only the system with 1 ML oxygen coverage has local magnetic moments. Atom resolved electronic density analysis revealed that the unpaired electrons are primarily localized on the oxygen atom which forms a longer O-W bond, and this surface oxygen atom carries about 1.5 unpaired electrons. Two of the four O atoms in the same plane as the W atoms are only slightly magnetized, each account for 0.25 electrons.

We also found that molecular oxygen may be formed and adsorbed on the surface when the oxygen coverage is larger than 0.5 ML, forming superoxide-like species. This finding is consistent with the photoelectron spectroscopic characterization of WO_x clusters[47] and may explain the structural disorder observed in the STM study of oxygen adsorption on WO_3(001) when oxygen coverage is larger than 0.5 monolayer.[45]

3.2 ReO_3 (001)

We then performed a similar analysis for oxygen on ReO_3(001) by starting with a nonstoichiometric ReO_2 terminated slab. The formation of the c(2×2) oxygen super structure, as shown by the blue square in fig. 2(b), on the basis of ReO_2 terminated surface is also exothermic, with integral heats of dissociative adsorption of -439.7 kJ/mol. At this oxygen coverage (0.5 ML), the terminal O-Re bond is 1.74 Å, similar to that on WO_3(001). The creation of the surface also makes the Re-O bonds along the surface normal alternate between long and short, although the extent of the oscillation is not as big as that on WO_3(001). Further increasing the oxygen coverage to 1 ML, i.e., covering all the surface Re atoms of the ReO_2 terminated surface, the

integral heats of dissociative adsorption became -361.1 kJ/mol with respect to the ReO_2 terminated slab and isolated O_2 molecules. This value is significantly larger than the corresponding value on WO_3(001). Consequently, dissociative adsorption of oxygen on ReO_3(001) is exothermic even if the 0.5 ML oxygen covered stoichiometric slab was used as a reference (-282.5 kJ/mol). The strong exothermicity of O_2 dissociative adsorption at 1 ML oxygen coverage indicates that it is feasible to maintain a high oxygen coverage on ReO_3(001). Furthermore, the relative small variation of oxygen adsorption energies upto 1 ML coverage suggests that ReO_3 may be used an oxygen carrier in oxidation reactions. Molecular O_2 adsorption on the surface with 0.5 ML O forming a c(2×2) oxygen super structure was also examined. The results showed that dissociative adsorption is significantly favorable over the molecular adsorption even at the full monolayer oxygen coverage. To the best of our knowledge, there have been no experimental studies of the surface structure based on well-defined ReO_3 single crystal as well as the dependence of the structure on oxygen partial pressures.

3.3 Methanol adsorption and dissociation on WO_3 (001)

Methanol adsorption and dissociation have been studied in both the c(2×2) and p(2×2) unit cells with 0.5 ML oxygen coverage on WO_3(001). The corresponding methanol coverages are 0.5 and 0.25 ML, respectively. Methanol adsorption energies were calculated as $\Delta E_{ads} = E_{Me/slab} - E_{slab} - E_{methanol}$, where $E_{Me/slab}$ is the energy of the slab with either molecularly or dissociatively adsorbed methanol, E_{slab} represents the energy of WO_3 (or ReO_3 in the following section) slab terminated with 0.5 ML oxygen, and $E_{methanol}$ is the energy of an isolated methanol molecule. The results were summarized in table 1.

The top and side views of a molecularly adsorbed methanol in a p(2×2) surface unit cell were shown in fig. 3. In this configuration, the oxygen atom of the methanol hydroxyl binds the surface W atom. The C-O and O-H bond distances in adsorbed methanol are 1.45 and 0.99 Å, respectively, and are only slightly longer than those calculated with an isolated methanol molecule (1.43 and 0.97 Å, respectively). The distance between of the methanol O to the surface W is 2.33 Å. This configuration also allows the formation of an O-H···O structure, with a H···O distance of 1.80 Å. The hydrogen bond-like structure helps to stabilize the molecularly adsorbed methanol. As shown in table 1, the adsorption energy for methanol calculated in a p(2×2) unit

cell is slightly larger than that in a c(2×2) unit cell, indicating a weak repulsive interactions between the molecularly adsorbed methanol as the coverage is increased.

Two dissociation channels: forming $CH_3O_{(a)}+H_{(a)}$ and $CH_2OH_{(a)}+H_{(a)}$ were analyzed. The dissociative adsorption energies with respect to an isolated methanol molecule were also listed in Table 1. Obviously, both dissociation channels are endothermic. In $CH_3O_{(a)}+H_{(a)}$, the hydrogen adatom occupies the neighboring surface oxygen site and forms a surface hydroxyl group, as shown in figure 4. This configuration with coadsorbed methoxide and H, circled in figure 4, can only be maintained by rotating the newly formed O-H bond away from the original plane. In fact, relaxation from adsorbed methoxide on W site and hydrogen adatom on the surface oxygen site with the newly formed O-H bond in the same plane as O-H···O led to H moving back to the O atom of the adsorbed methoxide and forming molecularly adsorbed methanol. The O-H bond in the surface hydroxyl is 0.97 Å. The C-O and O-W bond distances in the adsorbed methoxide are 1.40 and 1.93Å, respectively, shorter than the corresponding values in the molecularly adsorbed methanol.

An alternative pathway involves extracting hydrogen from the methyl group of methanol to form coadsorbed hydroxymethyl and hydrogen adatom, i.e., $CH_2OH_{(a)}+H_{(a)}$. In this configuration, CH_2OH binds to surface W atom through the C atom, forming a C-W bond of 2.35 Å. Similarly, the hydrogen adatom from the dehydrogenation forms a surface hydroxyl group with the terminal oxygen. The calculated dissociative adsorption energy for this product state shows that this channel is even more endothermic, with heats of reaction being 94.4 and 114.4 kJ/mol at 0.5 and 0.25 ML methanol coverage, respectively. Due to the high endothermicity of both reaction channels on WO_3(001), we did not perform transition state calculations for dissociation of adsorbed methanol.

3.4 Methanol adsorption and dissociation on ReO_3 (001)

In order to compare the reactivity of ReO_3 with WO_3, we examined methanol adsorption and dissociation only in a p(2×2) surface unit cell with 0.5 ML oxygen coverage. The top and side views of a molecularly adsorbed methanol in the p(2×2) surface unit cell were shown in fig. 5. Similar to methanol on WO_3(001), the oxygen atom of the methanol hydroxyl binds the surface Re atom. The C-O and O-H bond distances of adsorbed methanol on ReO_3(001) are almost the same as those on WO_3(001). The distance between of the methanol O to the surface Re is 2.21 Å,

shorter by 0.12 Å than the corresponding O-W distance. The H···O distance in the O-H···O structure on ReO_3(001) is 2.04 Å., significantly longer than that on WO_3(001). Molecular adsorption was found to be exothermic, with an adsorption energy of -106.4 kJ/mol.

We also examined two dissociation channels, i.e., forming $CH_3O_{(a)}+H_{(a)}$ and $CH_2OH_{(a)}+H_{(a)}$, on ReO_3(001). The dissociative adsorption energies with respect to an isolated methanol molecule were also listed in Table 1. Obviously, both dissociation channels are exothermic. In $CH_3O_{(a)}+H_{(a)}$, the hydrogen adatom occupies the neighboring surface oxygen site and forms a surface hydroxyl group, as shown in figure 6. In contrast to methanol dissociation on WO_3(001), the coadsorbed methoxide and H on ReO_3(001), circled in figure 6, is a minimum on the potential energy surface. The O-H bond in the surface hydroxyl is 0.98 Å. The C-O and O-Re bond distances in the adsorbed methoxide are 1.42 and 1.93Å. The H···O distance in the O-H···O structure is 2.42 Å.

We further explored the reaction pathways to form $CH_3O_{(a)}+H_{(a)}$ and searched for transition state along this path on ReO_3(001). Five images were interpolated between the molecularly adsorbed initial state (fig. 5) and the dissociative state (fig. 6). The transition state determined from these images by using NEB method was further optimized using quasi-Newton method. The final structure of the transition state is shown in figure 7 with the key structure parameters labeled. The H atom in the transition state is located almost in the middle of the surface and methanol O atoms, with distances being 1.195 and 1.267 Å, respectively. The barrier is only 19.1 kJ/mol with respective to the molecularly adsorbed methanol. This transition state is 87.3 kJ/mol lower than the energy of the gas phase methanol, suggesting that the molecularly and dissociatively adsorbed methanol must be in equilibrium on the surface. Therefore, operating conditions such as water vapor pressure will affect the surface coverage of hydroxyls, and in turn will determine relative abundance of surface molecular methanol and methoxide.

The pathway leading to the formation of coadsorbed hydroxymethyl and hydrogen adatom, i.e., $CH_2OH_{(a)}+H_{(a)}$, by extracting hydrogen from the methyl group of methanol, was found to be energetically favorable with respect to gas phase methanol molecule. CH_2OH binds to surface Re atom through the C atom and the C-Re bond is 2.18 Å. The hydrogen adatom from the dehydrogenation forms a surface hydroxyl group with the terminal oxygen and the O-H bond length is 1.01 Å. The dissociative adsorption energy for this product state is -23.7 kJ/mol.

Therefore, breaking C-H bond directly is possible on ReO_3(001) and will lead to a different product distribution for further oxidation of methanol.

3.5 **General Discussion**

Clearly, the reactivity of WO_3 and ReO_3 towards O-H and C-H bond cleavage in methanol is very different. On WO_3(001) with 0.5 ML oxygen, the heterolytic breaking of methanol O-H bond is clearly not favorable. In contrast, breaking O-H bond is energetically favorable on ReO_3(001). Even breaking C-H bond in methanol becomes feasible on ReO_3(001). In order to understand the difference between these two metal oxides surfaces, we analyzed the detailed local density of states of these adsorption systems. In figure 8, we plotted the local density of states of W and O in molecularly adsorbed methanol and adsorbed methoxide on WO_3(001). For comparison, we plotted in figure 9 the LDOS of Re and O for molecularly adsorbed methanol and adsorbed methoxide on ReO_3(001) as well as at the transition state of methanol dissociation in figure 9. The LDOS were plotted by aligning at the Fermi level of the corresponding system. Detailed analysis showed that the O 2p states at energies of -2.5 eV and -7 eV for CH_3OH/WO_3(001) and -4.5 eV and -9 eV for CH_3OH/ReO_3(001) are associated with the O-H bond of the adsorbed methanol. These states disappeared in the adsorbed methoxide on both oxide surfaces. We can see that the 2p levels of O are located at the top of the valence band for methanol on WO_3(001). The contribution of W at this level is not pronounced. Consequently, the coupling between the O 2p levels of methanol (methoxide) and W 5d is not strong. On ReO_3(001), the contribution to the states close to the Fermi level comes mainly from the 5d states of Re allowing for a better coupling with the energy levels of the O-H bond of methanol. The O 2p contribution is located at ~ -2 eV below Fermi level. Of course, the coverage of oxygen is expected to affect the surface chemistry of methanol. Increasing the oxygen coverage beyond 0.5 ML will likely reduce the sites available for methanol adsorption although the barrier for O—H bond breaking is not expected to change significantly as the process only involves the Re-bound methanol and the neighbouring terminal oxygen. On the other hand, other reaction channels such as C—O bond breaking may become accessible at lower oxygen coverages.

The molecular structures of the active metal oxide species are expected to play important roles as the heterogeneous catalytic reactions occur at the surfaces of catalysts.[48] There have been many studies attempted to relate the molecular structures of the supported metal oxide

species to their catalytic properties. Many physical characterization techniques have been developed to probe different aspects of the catalysts “off-situ” or “in-situ”. For example, Wachs and coworkers have employed Raman and IR to characterize a wide range of supported metal oxides including WO_x and ReO_x.[49] Their studies provided some useful insight into the molecular structures under different operating conditions. The degree of hydration of the metal oxide surfaces has strong influence on the reactions that require the acidic/basic sites on the surface.[50, 51] In fact, water adsorption and dissociation on these surfaces follow a similar trend to that of the methanol, i.e. H_2O favors molecular adsorption strongly on the perfect WO_3(001) whereas the molecularly and dissociatively adsorbed H_2O on ReO_3 have a similar stability. The affinities of the oxide surfaces to water and their ability to dissociatively adsorbed water have been shown to have a significant on the oxides as catalysts or support/promoters for a catalyst.[39, 52-55]

4. Conclusions

First principles density functional theory was used to analyze the adsorption and dissociation of methanol on the surfaces of two structurally similar transition metal oxides, WO_3(001) and ReO_3(001). The adsorption energies of molecularly adsorbed methanol on WO_3(001) and ReO_3(001) are -74.0 and -106.4 kJ/mol, respectively. On the other hand, dissociative adsorption of methanol to adsorbed methoxide species is not energetically favored on WO_3(001) but favored on ReO_3(001). The dissociation to form coadsorbed methoxide and hydrogen adatom has been found 34.8 kJ/mol endothermic on WO_3 and -111.2 kJ/mol exothermic on ReO_3, respectively. The activation barrier for the dissociation of molecularly adsorbed methanol on ReO_3(001) was determined to be 19.1 kJ/mol. Dehydrogenations to form coadsorbed hydroxymethyl and hydrogen adatom are not energetically favorable on both surfaces with respect to the molecularly adsorbed methanol. However, the reaction with respect to gas phase methanol is exothermic on ReO_3 with the heats of reaction of -23.7 kJ/mol but endothermic on WO_3 with the heat of reaction of 114.4 kJ/mol. We conclude that the differences between electronic and crystal structure of ReO_3 and WO_3 contribute to differences in chemical properties of the (001) surfaces of these trioxides.

Acknowledgements:

This work was supported by the Office of Basics Energy Sciences, U.S. Department of Energy (DOE) under grant No. DE-FG02-05ER46231. Calculations was done at the W. R. Wiley Environmental Molecular Sciences Laboratory (EMSL), a national scientific user facility sponsored by DOE's Office of Biological and Environmental Research and located at PNNL. PNNL is operated by Battelle for the U.S. DOE.

References

[1] Henrich, V. E.; Cox, P. A. *The Surface Science of Metal Oxides*; Cambridge University Press: Cambridge, 1996.

[2] Murrell, L. L.;Grenoble, D. C.;Kim, C. J.; Dispenziere, N. C. Supported Transition-Metal Oxides as Acid Cracking Catalysts - Periodic Trends and Their Relationship to Activity and Selectivity. *J. Catal.* 1987, *107*, 463-470.

[3] Benitez, V. M.;Querini, C. A.; Figoli, N. S. Characterization of WO_x/Al_2O_3 and MoO_x/Al_2O_3 catalysts and their activity and deactivation during skeletal isomerization of 1-butene. *Appl. Catal. A-Gen.* 2003, *252*, 427-436.

[4] Mamede, A. S.;Payen, E.;Grange, P.;Poncelet, G.;Ion, A.;Alifanti, M.; Parvulescu, V. I. Characterization of WO_x/CeO_2 catalysts and their reactivity in the isomerization of hexane. *J. Catal.* 2004, *223*, 1-12.

[5] Di Gregorio, F.; Keller, V. Activation and isomerization of hydrocarbons over WO_3/ZrO_2 catalysts - I. Preparation, characterization, and X-ray photoelectron spectroscopy studies. *J. Catal.* 2004, *225*, 45-55.

[6] Benitez, V. M.;Querini, C. A.;Figoli, N. S.; Comelli, R. A. Skeletal isomerization of 1-butene on WO_x/γ-Al_2O_3. *Appl. Catal. A-Gen.* 1999, *178*, 205-218.

[7] Ji, W. J.;Chen, Y.; Kung, H. H. Vapor phase aldol condensation of acetaldehyde on metal oxide catalysts. *Appl. Catal. A-Gen.* 1997, *161*, 93-104.

[8] Hilbrig, F.;Schmelz, H.;Knozinger, H.;Sinev, M.;Bell, A. T.;Schmal, M.;Forzatti, P.;Wachs, I. E.;Uematsu, T.;Vedrine, J. C.; Hums, E. Acidity of WO_x/TiO_2 Catalysts for Selective Catalytic Reduction (SCR). *Studies in Surface Science and Catalysis* 1993, *75*, 1351-1362.

[9] Yuan, Y. H.; Iwasawa, Y. Performance and characterization of supported rhenium oxide catalysts for selective oxidation of methanol to methylal. *J. Phys. Chem. B* 2002, *106*, 4441-4449.

[10] Viswanadham, N.;Shido, T.; Iwasawa, Y. Performances of rhenium oxide-encapsulated ZSM-5 catalysts in propene selective oxidation/ammoxidation. *Appl. Catal. A* 2001, *219*, 223-233.

[11] Barton Cole, E.;Lakkaraju, P. S.;Rampulla, D. M.;Morris, A. J.;Abelev, E.; Bocarsly, A. B. Using a One-Electron Shuttle for the Multielectron Reduction of CO_2 to Methanol: Kinetic, Mechanistic, and Structural Insights. *J. Am. Chem. Soc.* 2010, *132*, 11539-11551.

[12] Ge, Q. Chapter 3 - Mechanistic Understanding of Catalytic CO_2 Activation from First Principles Theory. In *New and Future Developments in Catalysis*. Elsevier; Amsterdam, 2013; pp 49-79.
[13] Wachs, I. E.;Deo, G.;Juskelis, M. V.; Weckhuysen, B. M. Methanol oxidation over supported vanadium oxide catalysts: New fundamental insights about oxidation reactions over metal oxide catalysts from transient and steady state kinetics. In *Dynamics of Surfaces and Reaction Kinetics in Heterogeneous Catalysis*. 1997; pp 305-314.
[14] Cheng, W.-H.; Kung, H. H. *Methanol Production and Use*; Marcel Dekker: New York 1994.
[15] Badlani, M.; Wachs, I. E. Methanol: a "smart" chemical probe molecule. *Catal. Lett.* 2001, *75*, 137-149.
[16] Burcham, L. J.; Wachs, I. E. The origin of the support effect in supported metal oxide catalysts: in situ infrared and kinetic studies during methanol oxidation. *Catal. Today* 1999, *49*, 467-484.
[17] Wachs, I. E.;Chen, Y.;Jehng, J. M.;Briand, L. E.; Tanaka, T. Molecular structure and reactivity of the Group V metal oxides. *Catal. Today* 2003, *78*, 13-24.
[18] Gao, X. T.;Jehng, J. M.; Wachs, I. E. In situ UV-vis-NIR diffuse reflectance and Raman spectroscopic studies of propane oxidation over ZrO_2-supported vanadium oxide catalysts. *J. Catal.* 2002, *209*, 43-50.
[19] Schirber, J. E.; Morosin, B. "Compressibility Collapse" Transition in ReO_3. *Phys. Rev. Lett.* 1979, *42*, 1485-1487.
[20] Woodward, P. M.;Sleight, A. W.; Vogt, T. Ferroelectric Tungsten Trioxide. *Journal of Solid State Chemistry* 1997, *131*, 9-17.
[21] Butler, M. A.;Nasby, R. D.; Quinn, R. K. Tungsten trioxide as an electrode for photoelectrolysis of water. *Solid State Communications* 1976, *19*, 1011-1014.
[22] Ferretti, A.;Rogers, D. B.; Goodenough, J. B. The relation of the electrical conductivity in single crystals of rhenium trioxide to the conductivities of Sr_2MgReO_6 and Na_xWO_3. *Journal of Physics and Chemistry of Solids* 1965, *26*, 2007-2011.
[23] Gurlo, A. Nanosensors: towards morphological control of gas sensing activity. SnO_2, In_2O_3, ZnO and WO_3 case studies. *Nanoscale* 2011, *3*, 154-165.
[24] Mei, D.;Deskins, N. A.;Dupuis, M.; Ge, Q. Density Functional Theory Study of Methanol Decomposition on the CeO_2(110) Surface. *J. Phys. Chem. C* 2008, *112*, 4257-4266.
[25] Mei, D.;Deskins, N. A.;Dupuis, M.; Ge, Q. Methanol Adsorption on the Clean CeO_2(111) Surface: A Density Functional Theory Study. *J. Phys. Chem. C* 2007, *111*, 10514-10522.
[26] Han, Y.;Liu, C.-j.; Ge, Q. Effect of Pt Clusters on Methanol Adsorption and Dissociation over Perfect and Defective Anatase TiO_2(101) Surface. *J. Phys. Chem. C* 2009, *113*, 20674-20682.
[27] Ye, J.;Liu, C.; Ge, Q. A DFT study of methanol dehydrogenation on the PdIn(110) surface. *Phys. Chem. Chem. Phys.* 2012, *14*, 16660-16667.
[28] Kresse, G.; Hafner, J. Ab initio Molecular-Dynamics for Liquid-Metals. *Phys. Rev. B* 1993, *47*, 558-561.
[29] Kresse, G.; Furthmuller, J. Efficiency of ab-initio total energy calculations for metals and semiconductors using a plane-wave basis set. *Comput. Mater. Sci.* 1996, *6*, 15-50.
[30] Vanderbilt, D. Soft Self-Consistent Pseudopotentials in a Generalized Eigenvalue Formalism. *Phys. Rev. B* 1990, *41*, 7892-7895.

[31] Blochl, P. E. Projector Augmented-Wave Method. *Phys. Rev. B* 1994, *50*, 17953-17979.
[32] Hobbs, D.;Kresse, G.; Hafner, J. Fully unconstrained noncollinear magnetism within the projector augmented-wave method. *Phys. Rev. B* 2000, *62*, 11556-11570.
[33] Perdew, J. P.;Chevary, J. A.;Vosko, S. H.;Jackson, K. A.;Pederson, M. R.;Singh, D. J.; Fiolhais, C. Atoms, Molecules, Solids, and Surfaces - Applications of the Generalized Gradient Approximation for Exchange and Correlation. *Phys. Rev. B* 1992, *46*, 6671-6687.
[34] Perdew, J. P.;Burke, K.; Ernzerhof, M. Generalized gradient approximation made simple. *Phys. Rev. Lett.* 1996, *77*, 3865-3868.
[35] Monkhorst, H. J.; Pack, J. D. Special points for Brillouin-zone integrations. *Phys. Rev. B* 1976, *13*, 5188-5192.
[36] Mills, G.;Jonsson, H.; Schenter, G. K. Reversible Work Transition-State Theory - Application to Dissociative Adsorption of Hydrogen. *Surf. Sci.* 1995, *324*, 305-337.
[37] Henkelman, G.; Jonsson, H. Improved tangent estimate in the nudged elastic band method for finding minimum energy paths and saddle points. *J. Chem. Phys.* 2000, *113*, 9978-9985.
[38] Henkelman, G.;Uberuaga, B. P.; Jonsson, H. A climbing image nudged elastic band method for finding saddle points and minimum energy paths. *J. Chem. Phys.* 2000, *113*, 9901-9904.
[39] Pan, Y.-x.;Liu, C.-j.; Ge, Q. Effect of surface hydroxyls on selective CO_2 hydrogenation over Ni_4/γ-Al_2O_3: A density functional theory study. *J. Catal.* 2010, *272*, 227-234.
[40] Ye, J.;Liu, C.-j.;Mei, D.; Ge, Q. Methanol synthesis from CO_2 hydrogenation over a Pd_4/In_2O_3 model catalyst: A combined DFT and kinetic study. *J. Catal.* 2014, *317*, 44-53.
[41] Kresse, G.; Furthmuller, J. VASP, the Guide. 2005.
[42] Schirber, J. E.; Morosin, B. "Compressibility Collapse" Transition in ReO_3. *Phys. Rev. Lett.* 1979, *42*, 1485.
[43] Woodward, P. M.; Sleight, A. W. Ferroelectric Tungsten Trioxide. *Journal of Solid State Chemistry* 1997, *131*, 9-17.
[44] Yakovkin, I. N.; Gutowski, M. Driving force for the WO_3(001) surface relaxation. *Surface Science* 2007, *601*, 1481-1488.
[45] Tanner, R. E.; Altman, E. I. Effect of surface treatment on the γ-WO_3(001) surface: A comprehensive study of oxidation and reduction by scanning tunneling microscopy and low-energy electron diffraction. *Journal of Vacuum Science & Technology A* 2001, *19*, 1502-1509.
[46] Li, M.;Posadas, A.;Ahn, C. H.; Altman, E. I. Scanning tunneling microscopy study of terminal oxygen structures on WO_3(100) thin films. *Surface Science* 2005, *579*, 175-187.
[47] Huang, X.;Zhai, H. J.;Li, J.; Wang, L. S. On the structure and chemical bonding of tri-tungsten oxide clusters $W_3O_n^-$ and W_3O_n (n=7-10): W_3O_8 as a potential molecular model for O-deficient defect sites in tungsten oxides. *J. Phys. Chem. A* 2006, *110*, 85-92.
[48] Ling, S.;Mei, D.; Gutowski, M. Reactivity of hydrogen and methanol on (001) surfaces of WO_3, ReO_3, WO_3/ReO_3 and ReO_3/WO_3. *Catal. Today* 2011, *165*, 41-48.
[49] Wachs, I. E. Raman and IR studies of surface metal oxide species on oxide supports: Supported metal oxide catalysts. *Catal. Today* 1996, *27*, 437-455.
[50] Macht, J.;Baertsch, C. D.;May-Lozano, M.;Soled, S. L.;Wang, Y.; Iglesia, E. Support effects on Bronsted acid site densities and alcohol dehydration turnover rates on tungsten oxide domains. *J. Catal.* 2004, *227*, 479-491.

[51] Onfroy, T.;Clet, G.; Houalla, M. Acidity, surface structure, and catalytic performance of WOx supported on monoclinic zirconia. *J. Phys. Chem. B* 2005, *109*, 3345-3354.
[52] Pan, Y.;Liu, C.-j.; Ge, Q. Adsorption and Protonation of CO_2 on Partially Hydroxylated γ-Al_2O_3 Surfaces: A Density Functional Theory Study. *Langmuir* 2008, *24*, 12410-12419.
[53] Pan, Y.-x.;Kuai, P.;Liu, Y.;Ge, Q.; Liu, C.-j. Promotion effects of Ga_2O_3 on CO_2 adsorption and conversion over a SiO_2-supported Ni catalyst. *Energy & Environmental Science* 2010, *3*, 1322-1325.
[54] Pan, Y.-x.;Liu, C.-j.;Mei, D.; Ge, Q. Effects of Hydration and Oxygen Vacancy on CO_2 Adsorption and Activation on β-Ga_2O_3(100). *Langmuir* 2010, *26*, 5551-5558.
[55] Yin, S.;Swift, T.; Ge, Q. Adsorption and activation of CO_2 over the Cu-Co catalyst supported on partially hydroxylated γ-Al_2O_3. *Catalysis Today* 2011, *165*, 10-18.

Table 1. DFT GGA calculated adsorption energies of molecular and dissociative adsorption on WO_3(001) and ReO_3(001)

	WO_3(001)		ReO_3(001)
	c(2x2) (kJ/mol)	p(2x2) (kJ/mol)	p(2x2) (kJ/mol)
$CH_3OH_{(a)}$	-74.1	-74.0	-106.4
$CH_3O_{(a)}+H_{(a)}$	15.0	34.8	-111.2
$CH_2OH_{(a)}+H_{(a)}$	94.4	114.4	-23.7

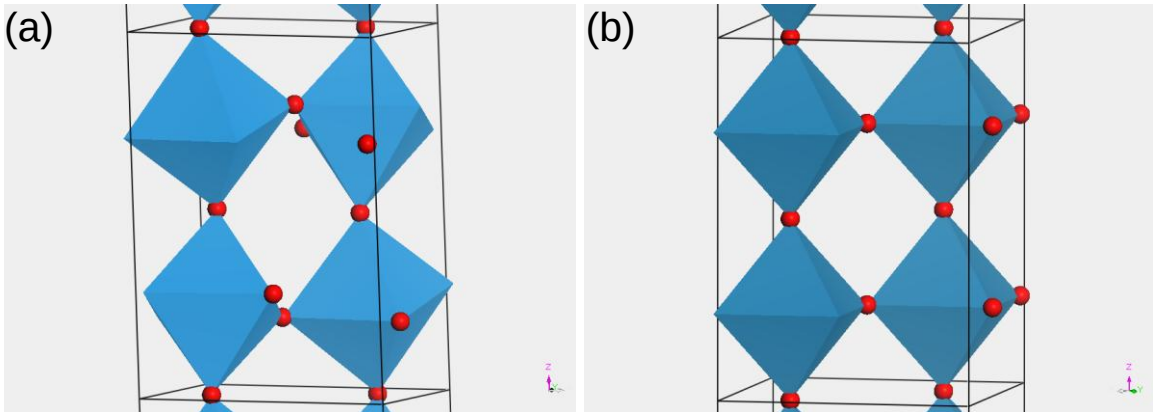

Fig. 1. Ployhedron representation of the relaxed bulk structures of (a) ε-WO_3 and (b) ReO_3.

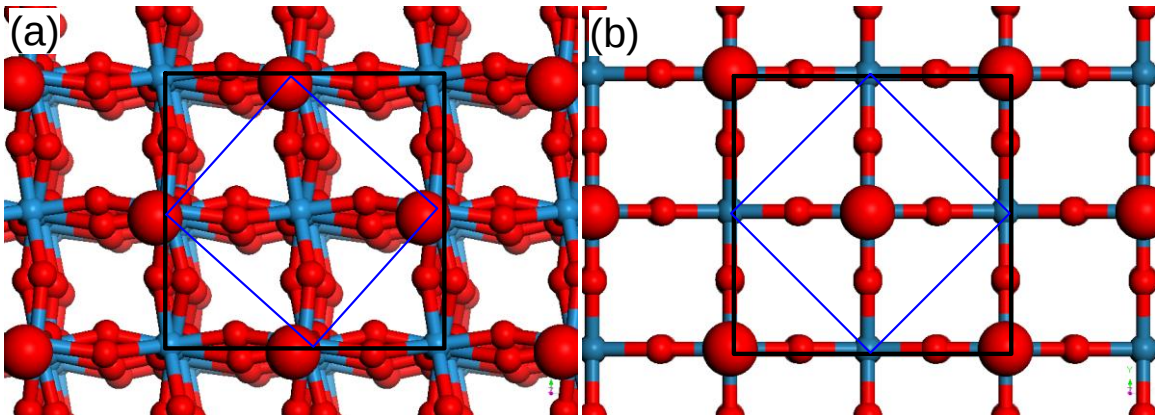

Fig. 2. Top view of the surface c(2×2) (blue) and p(2×2) (black) unit-cells of (a) ε-WO_3(001) and (b) ReO_3(001). Color code: Red – Oxygen; Blue – W or Re. Large red spheres represent surface oxygen atoms.

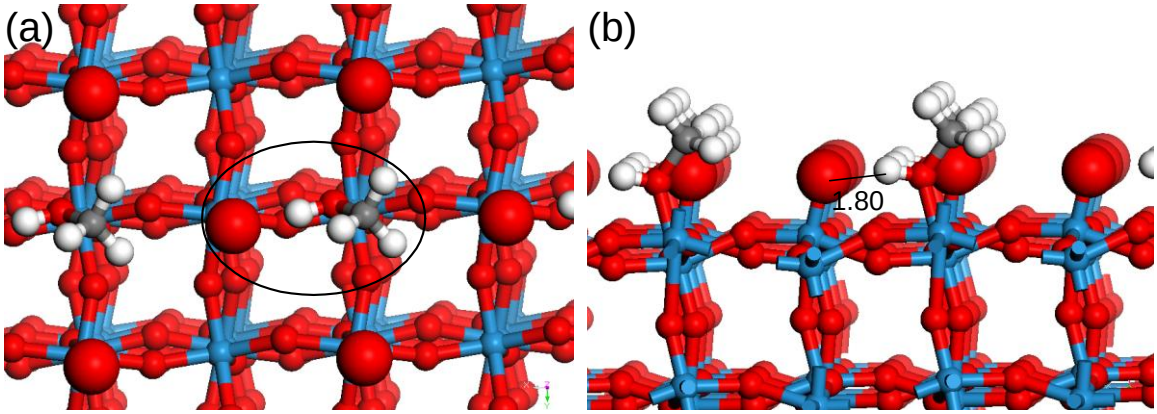

Fig. 3. Top view, (a), and side view, (b), of methanol molecularly adsorbed on ε-WO_3(001), respectively. Color code: Red – Oxygen; Blue – W or Re; Dark grey – Carbon; White - Hydrogen. Large red spheres represent surface oxygen atoms. The adsorbed methanol and the neighboring O atom are circled.

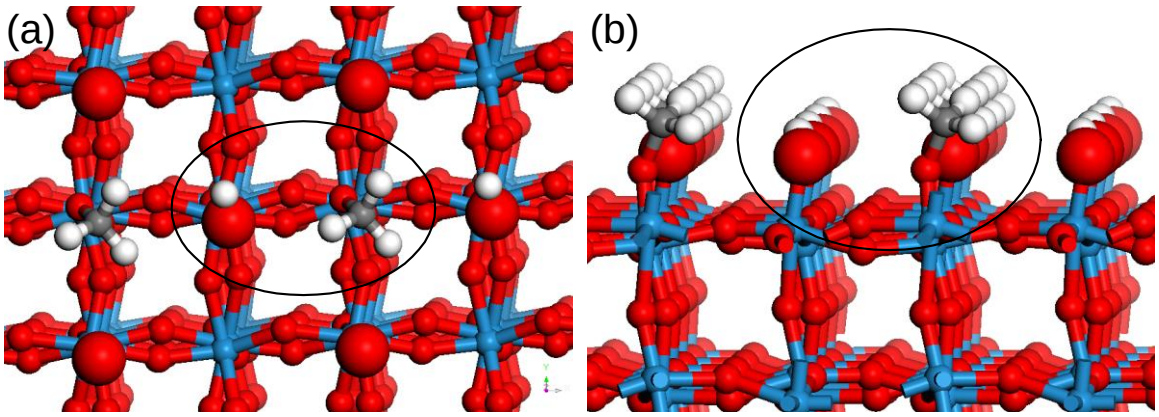

Fig. 4. Top view, (a), and side view, (b), of methanol dissociative adsorption on ε-WO_3(001), respectively. See Figure 3 for color code. The adsorbed methoxide and the neighboring surface hydroxyl are circled.

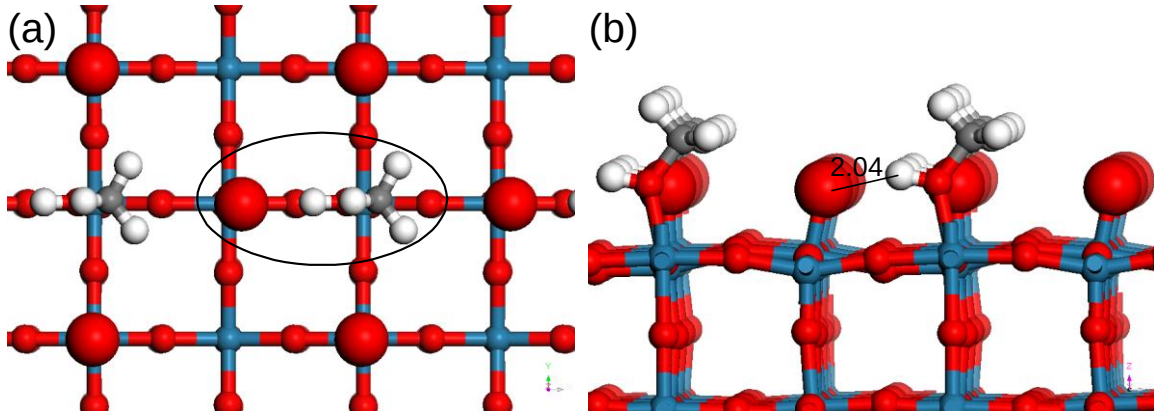

Fig. 5. Top view, (a), and side view, (b), of methanol molecular adsorption on ReO_3(001), respectively. See Figure 3 for color code. The adsorbed methanol and the neighboring surface O atom are circled in (a).

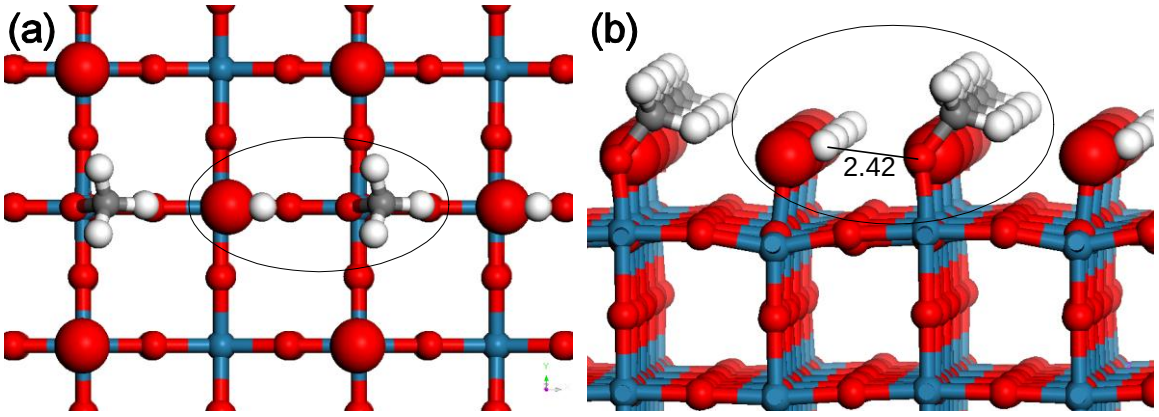

Fig. 6. Top view, (a), and side view, (b), of dissociative adsorption of methanol on ReO_3(001), respectively. See Figure 3 for color code. The adsorbed methoxide and the neighboring surface hydroxyl are circled.

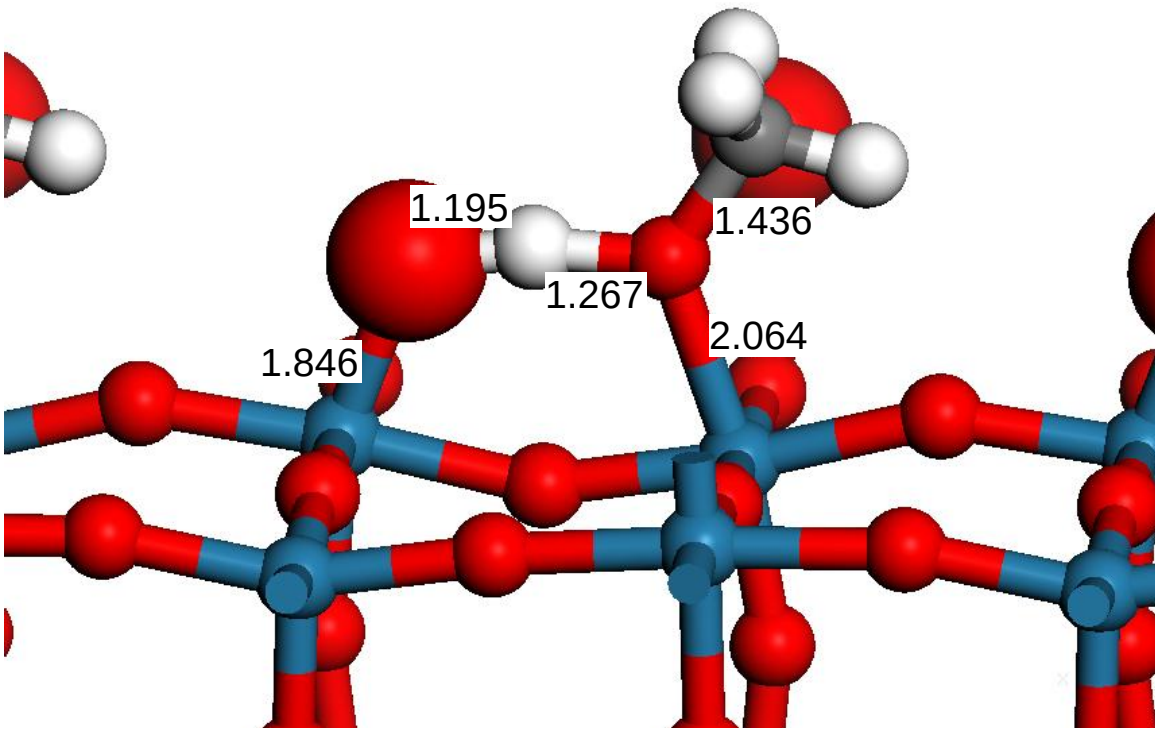

Fig. 7. Transition state structure for methanol dissociation on ReO_3(001). See Figure 3 for color code.

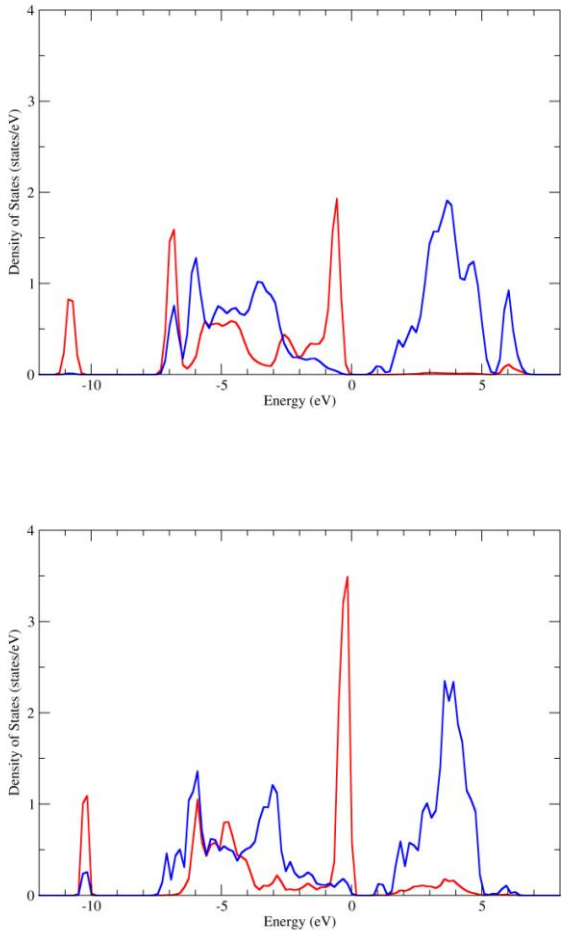

Fig. 8. Local density of states plots of O (red) and W (blue) in molecularly adsorbed methanol (upper) and adsorbed methoxide (lower).

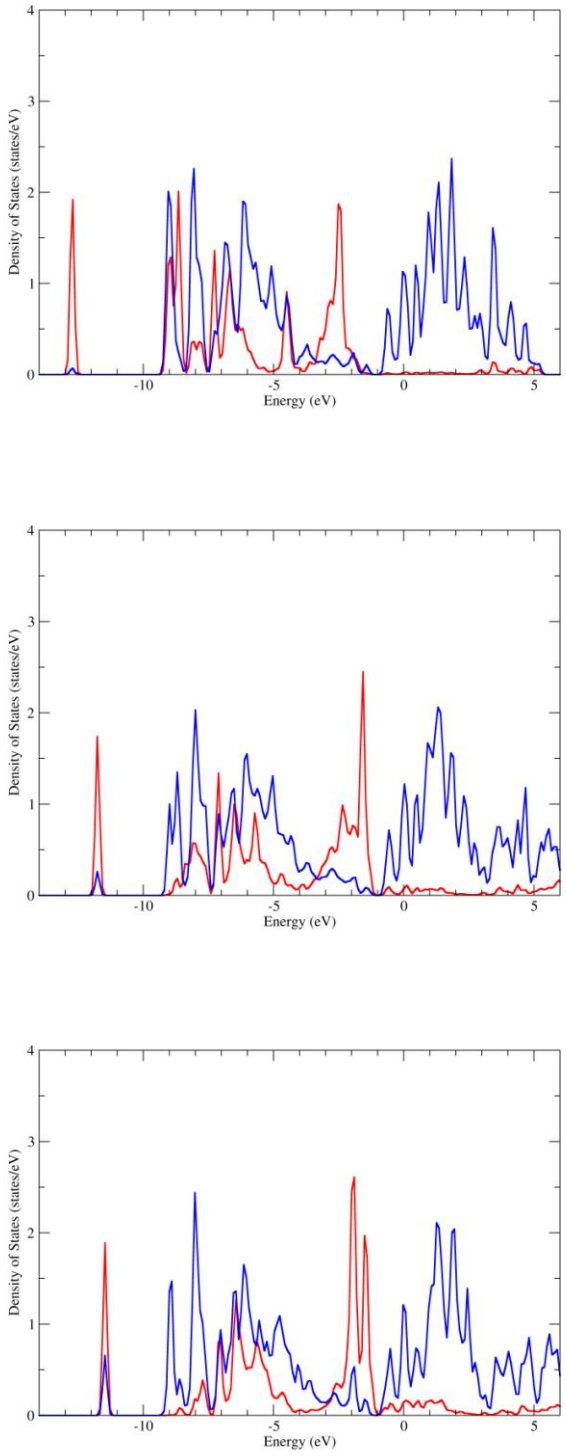

Fig. 9. Local density of states plots of O (red) and Re (blue) in molecularly adsorbed methanol (top), transition state (middle), and adsorbed methoxide (bottom). Zero on x-axis corresponds to Fermi energy.